

Preparation of $\text{Fe}_3\text{O}_4@$ APTES-TA-MA covalent organic framework nanocatalyst for the construction of N-amino-2-pyridone analogs

Amaneh Mosaffaeirad , Masoud Mokhtary* , Mohammad Nikpassand 

Department of Chemistry, Rasht Branch, Islamic Azad University, Rasht, Iran.

*Corresponding author: mmokhtary@iaurasht.ac.ir

Review Paper

Received:

22 January 2024

Revised:

28 February 2024

Accepted:

10 March 2024

Published online:

29 March 2024

Abstract:

In this work, an efficient method for the construction of N-amino-2-pyridone analogs was performed using the condensation of aldehyde, malononitrile and cyanoaceto-hydrazide through $\text{Fe}_3\text{O}_4@$ aminopropyltriethoxysilane-terephthalaldehyde-melamine ($\text{Fe}_3\text{O}_4@$ APTES-TA-MA) as an efficient recyclable magnetic covalent organic framework nanocatalyst in ethanol at reflux conditions. $\text{Fe}_3\text{O}_4@$ APTES-TA-MA was characterized via FT-IR, EDS, SEM, TEM, VSM, and TGA methods. The average size of the nanoparticles was found between 40-90 nm. Clean procedure, short reaction time, and high efficiency are some benefits of this protocol. Also, the nanomagnetic catalyst can be reused five times without significant loss of its activity.

© The Author(s) 2024

Keywords: Covalent organic frameworks; Cyanoaceto-hydrazide; Magnetic catalyst; N-Amino-2-pyridone

1. Introduction

Covalent organic frameworks (COFs) are novel crystalline polymers with well-defined frameworks and nanopores mainly composed of lightweight elements (H, B, C, N, and O) linked by dynamic covalent bonds that were first reported by Yaghi et al. [1, 2] COFs possess attractive features, such as large surface area, predesignable pore geometry, inherent adaptability, high crystallinity, and good flexibility. Their tunable porosity, large surface area, and π conjugation, with unique photoelectronic properties, enable COFs to serve as a promising platform for various applications.

Recently, magnetic nanoparticles-supported catalysts have increased attention in catalytic reactions and separation technologies due to high specific surface areas, highly dispersible in solvents, and superparamagnetic properties. Furthermore, catalysts immobilized on magnetic nanoparticles can be reused many times by simple magnetic attraction without considerable loss in their catalytic activity [3–16]. An additional interesting improvement is the poly(ionic liquids) stabilized magnetic nanoparticles as a new group of

heterogeneous nanocatalysts that is mainly attractive in organic synthesis practiced in an ecologically friendly way [17–19]. 2-Pyridone as a six-membered heterocyclic ring due to strong biological activities such as anti-bacterial [20], anti-tumor [21], anti-inflammatory [22], anti-proliferative [23], anti-hepatitis B virus [24], SARS-CoV-2 protease inhibitor [25], and analgesic [26] have attracted the attention of researchers. Also, 2-pyridone building blocks in the synthesis of alkaloids were reported as an essential class of natural organic compounds [27]. Figure 1 shows some 2-pyridone derivatives with significant antimicrobial properties [28].

Because of cyanoaceto-hydrazide chemical reactivity, cyanoaceto-hydrazide forms valuable synthetic units that give rise to many useful groups of organic compounds [29]. The construction of 2-pyridones has been reported via K_2CO_3 [30], bipyridinium chlorochromate [31], MgO and $\text{Bi}(\text{NO}_3)_3 \cdot 5\text{H}_2\text{O}$ [32], piperidine [33], Et_3N [34], nano- $\text{CdZr}_4(\text{PO}_4)_6$ [35], $\text{KF-Al}_2\text{O}_3$ [36], and ZnO NPs [37]. However, some of the reported methods have disadvantages, including the use of toxic and non-reusable catalysts, harsh

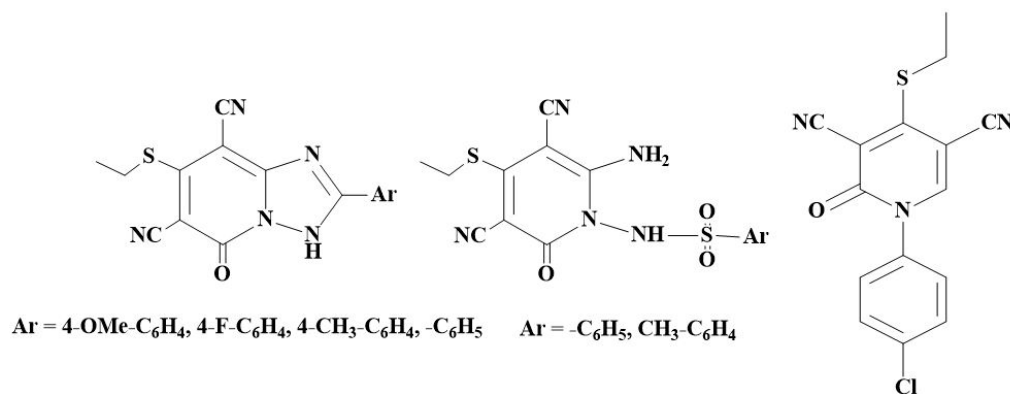


Figure 1. 2-Pyridone derivatives with significant antimicrobial agents.

reaction conditions, and long reaction times. Therefore, to overcome these restrictions, the discovery of a reusable and efficient catalyst with good catalytic activity for the production of 2-pyridones is still of interest. Following our research interest in the synthesis of cyanoacetohydrazide analogs and the desire to new methods for use in multicomponent reactions [38, 39], herein, an effective method for the production of N-amino-2-pyridone analogs has been developed by the one-step condensation of arylaldehyde, malononitrile and cyanoacetohydrazide using Fe₃O₄@APTES-TA-MA as an efficient basic recyclable magnetic covalent organic framework nanocatalyst in EtOH at reflux conditions (Scheme 1). It should be mentioned that the three derivatives 4e, 4h, and 4i were reported for the first time in this research.

2. Experimental

2.1 General

The chemical materials were prepared by Merck. The products were characterized by NMR spectra on a Bruker (Avance DRX-300 MHz) instrument. FT-IR spectra were determined by Shimadzu, SP-1100, P-UV-Com as KBr disk. TGA analysis was measured at a heating rate of 5 °C/min in the temperature range of 25 to 600 °C in the N₂ atmosphere by a Mettler Toledo apparatus. SEM image was obtained on a VEGA microscope. TEM micrograph was performed by

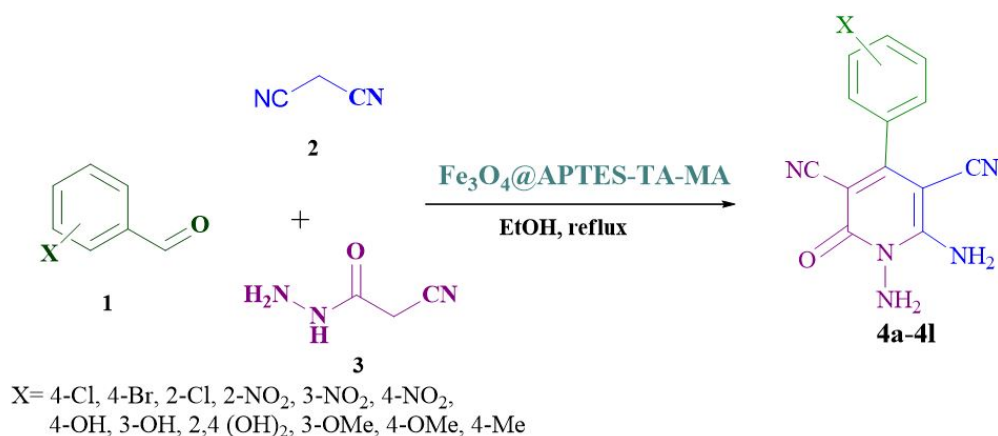
a Philips CM120 analyzer at 100 kV. XRD was run using a Philips, PW1730 diffractometer with Cu-K α radiation ($\lambda = 1.54 \text{ \AA}$).

2.2 Preparation of Fe₃O₄@APTES

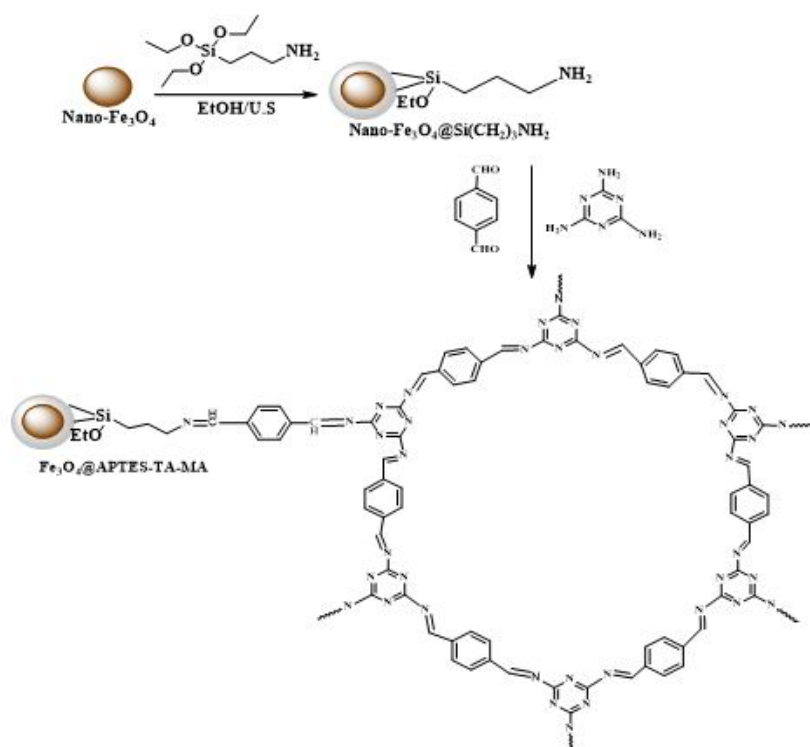
0.3 g of Fe₃O₄ was dispersed into a mixture of 4 mL deionized water and 600 mL absolute EtOH by ultrasonic vibration for 30 min. Then, APTES (1.2 mL) was added into the mixture under mechanical stirring for 7 h. The resulting Fe₃O₄ functionalized APTES nanoparticles were isolated by a magnet, then washed with EtOH and dried at 70 °C under vacuum for 24 h.

2.3 Preparation of Fe₃O₄@APTES-TA-MA

To a mixture of dioxane and toluene (1:1 v/v, 6 mL) were added Fe₃O₄@APTES (0.08 g), melamine (0.05 g), and terephthalaldehyde (0.04 g), and the mixture was ultrasonicated for 15 min. Subsequently, acetic acid (1.6 mL) was slowly added with sonication, and the resulting solution was placed in a 150 mL Teflon-lined autoclave and heated at 180 °C for 12h. After cooling down to room temperature, The Fe₃O₄@APTES-TA-MA precipitates were separated from the solution by an external magnetic field, followed by washing with ethanol several times. Finally, the Fe₃O₄@APTES-TA-MA were dried at 70 °C for further use.



Scheme 1. Production of N-amino-2-pyridone analogs catalyzed by Fe₃O₄@APTES-TA-MA.



Scheme 2. Schematic illustration of the $\text{Fe}_3\text{O}_4@APTES\text{-TA-MA}$.

2.4 General procedure for the construction of N-amino-2-pyridone analogs

A mixture of malononitrile (1.1 mmol), cyanoacetohydrazide (1 mmol), arylaldehyde (1 mmol), and $\text{Fe}_3\text{O}_4@APTES\text{-TA-MA}$ (0.04 g) was stirred at reflux conditions in EtOH (5 mL) for the 25-50 minutes. After completion of the reaction, the mixture was cooled to 25 °C, and the catalyst was separated by an external magnet. The crude product was recrystallized by EtOH to get pure products in 87-97% yields. All compounds were characterized by FT-IR, NMR, and melting point.

The spectroscopic data for product 4a

1,6-Diamino-4-(4-chlorophenyl)-2-oxo-1,2-dihydropyridine-3,5-dicarbonitrile (4a). Light yellow solid, yield (97%), FT-IR (KBr, cm^{-1}): ν_{max} = 3407, 2164, 1620, 1483, 1398, 1166, 1085, 819; ^1H NMR (DMSO d_6 , 300 MHz): δ 5.40 (s, 2H, N-NH₂), 7.59 (d, J = 8.1 Hz, 2H, ArH), 7.91 (d, J = 8.1 Hz, 2H), 8.74 (s, 2H, NH₂); ^{13}C NMR (DMSO d_6 , 75 MHz): δ 75.8 (C-CN), 85.2 (C-CN), 115.2 (CN), 116.5 (CN), 117.2, 129.5, 130.5, 133.0, 136.5, 157.5, 159.4, 159.8, 161.1 (C=O).

Full experimental detail, ^1H , and ^{13}C NMR spectra of all products can be found via the ‘‘Supplementary Information’’ section of this article’s webpage.

3. Results and discussion

In this work, $\text{Fe}_3\text{O}_4@APTES\text{-TA-MA}$ was prepared by the reaction $\text{Fe}_3\text{O}_4@APTES$, terephthalaldehyde, and melamine as depicted in Scheme 2. This organic modification on the surface of magnetic nanoparticles was realized by ap-

plying the layer-by-layer fabrication method depicted in Scheme 1. The Fe_3O_4 nanoparticles were initially reacted with (3-aminopropyl)triethoxysilane (APTES) to produce $\text{Fe}_3\text{O}_4@APTES$ nanoparticles. Later, the terephthalaldehyde, and melamine were added to react with the amino groups of $\text{Fe}_3\text{O}_4@APTES$. Subsequently, the $\text{Fe}_3\text{O}_4@APTES\text{-TA-MA}$ was fabricated as a basic magnetic covalent organic framework nanocatalyst.

Analysis functional groups of $\text{Fe}_3\text{O}_4@APTES\text{-TA-MA}$ were accomplished by FT-IR spectrum. According to the FT-IR characterization of $\text{Fe}_3\text{O}_4@APTES\text{-TA-MA}$, the stretching vibrations of NH and aromatic C-H were observed at 3340 and 3105 cm^{-1} respectively. The C=N and C=C stretching vibrations were observed at 1615 cm^{-1} and 1506 cm^{-1} respectively [40]. The C-N stretching vibration were observed at 1367 cm^{-1} . The Fe-O-Fe stretching vibrations were detected at 580 cm^{-1} (Figure 2(B)). These results provided evidence that terephthalaldehyde-melamine is successfully attached to $\text{Fe}_3\text{O}_4@APTES$.

The thermal analysis of $\text{Fe}_3\text{O}_4@APTES\text{-TA-MA}$ illustrated two main decreasing peaks (Fig. 3). The first reducing peak at a temperature of about 80-135 °C is related to the elimination of water from the surface of $\text{Fe}_3\text{O}_4@APTES\text{-TA-MA}$. The second reducing peak takes place at temperature up to 327 °C due to the degradation of the TA-MA from the catalyst. Thermal characterization data of $\text{Fe}_3\text{O}_4@APTES\text{-TA-MA}$ showed that the catalyst is stable to 300 °C.

Morphological study of the $\text{Fe}_3\text{O}_4@APTES\text{-TA-MA}$ surface was investigated by SEM (Fig. 4). The scanning electron microscopy image of the $\text{Fe}_3\text{O}_4@APTES\text{-TA-MA}$ displays a porous microstructure with cauliflower shapes

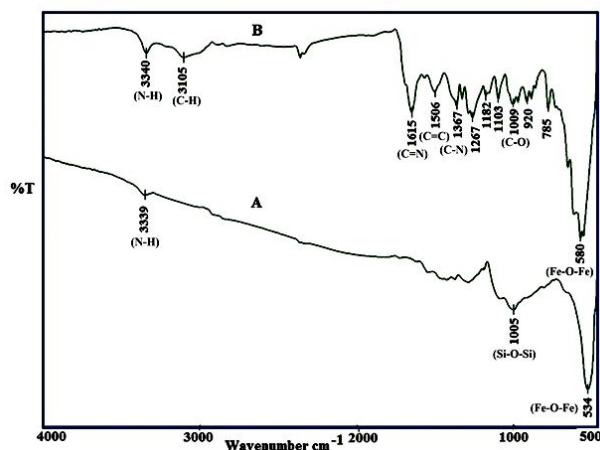


Figure 2. FT-IR spectra of: (A) Fe_3O_4 @APTES, (B) Fe_3O_4 @APTES-TA-MA.

with an average particle size of about 100 nm.

The elemental composition of the SEM of Fe_3O_4 @APTES-TA-MA image is shown in Fig. 5(a). The EDS spectrum shows the presence of C, N, O, Si and Fe atoms in Fe_3O_4 @APTES-TA-MA. Furthermore, the results of FE-SEM/mapping are presented in Fig. 5(b). As seen in Fig. 5, C, N, O, Si and Fe elements are uniformly dispersed in the catalyst structure.

The TEM micrograph of Fe_3O_4 @APTES-TA-MA was investigated to study its particle topology, distribution and size. TEM image of Fe_3O_4 @APTES-TA-MA shows a quasi-cube structure with low aggregation (Fig.6). The particles of Fe_3O_4 @APTES-TA-MA were observed approximately 40-90 nm with good dispersion (Fig.6(b)).

The magnetic property of Fe_3O_4 NPs, Fe_3O_4 @APTES NPs and Fe_3O_4 @APTES-TA-MA nanocatalyst was studied by VSM at ambient temperature (Fig. 7). According to the vibrating sample magnetometer spectrum of the catalyst, it can be seen that the magnetic property of the catalyst by increasing the magnetic strength of the external field, has increased and reached the saturation level in the field of about 5000. Saturation magnetization of Fe_3O_4 NPs, Fe_3O_4 @APTES NPs and Fe_3O_4 @APTES-TA-MA

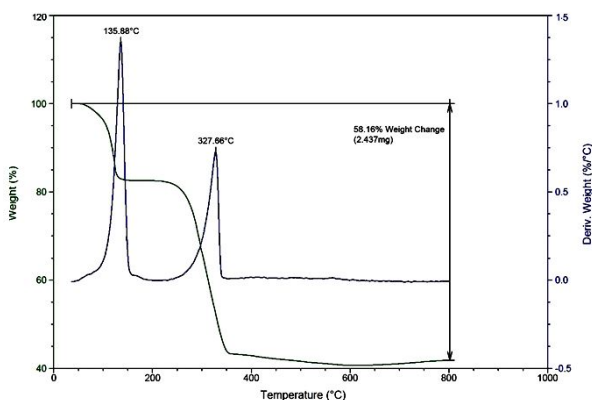


Figure 3. Thermal analysis diagram of Fe_3O_4 @APTES-TA-MA.

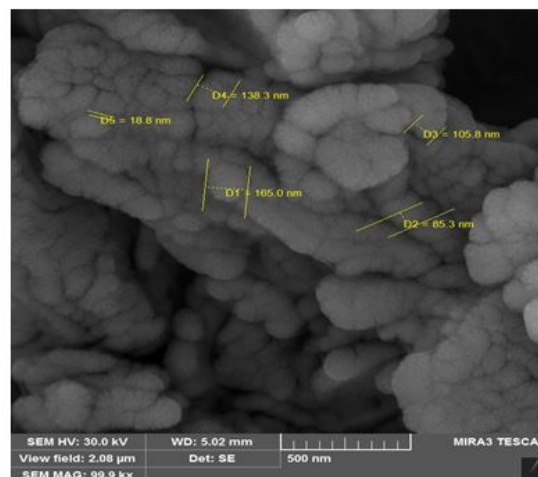


Figure 4. SEM image of Fe_3O_4 @APTES-TA-MA.

nanocatalyst was 48.9 emu g^{-1} , 42.9 emu g^{-1} , and 19.40 emu g^{-1} respectively. Compared with the Fe_3O_4 nanoparticles, the saturation magnetization of the Fe_3O_4 @APTES-TA-MA nanocatalyst obviously decreased due to the diamagnetic contribution of the thick SiO_2 and organic compounds. But, the magnetic saturation of Fe_3O_4 @APTES-TA-MA is a good number and shows that the nanocatalyst has good magnetic properties. The XRD patterns of Fe_3O_4 @APTES and Fe_3O_4 @APTES-TA-MA are presented in Fig. 8. The XRD model of the Fe_3O_4 @APTES-TA-MA demonstrated that the diffraction peaks were in match with the harmonic model of Fe_3O_4 @APTES [41].

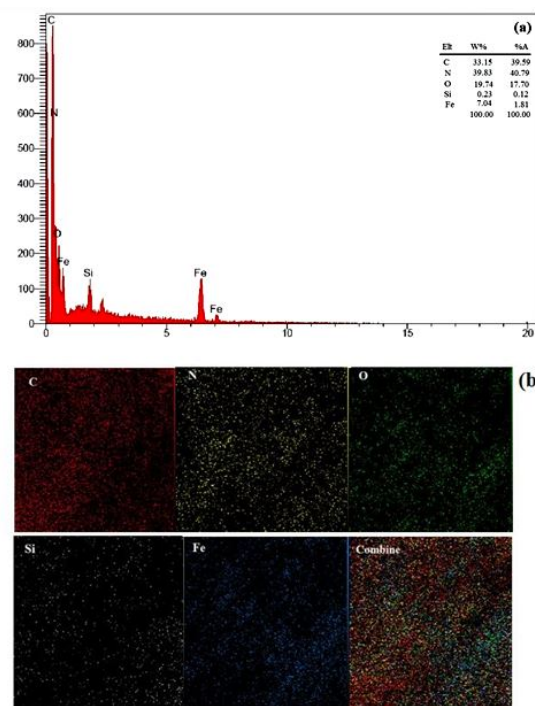


Figure 5. EDX (a) spectrum and Elemental mapping (b) of the C, N, O, Si and Fe elements of Fe_3O_4 @APTES-TA-MA.

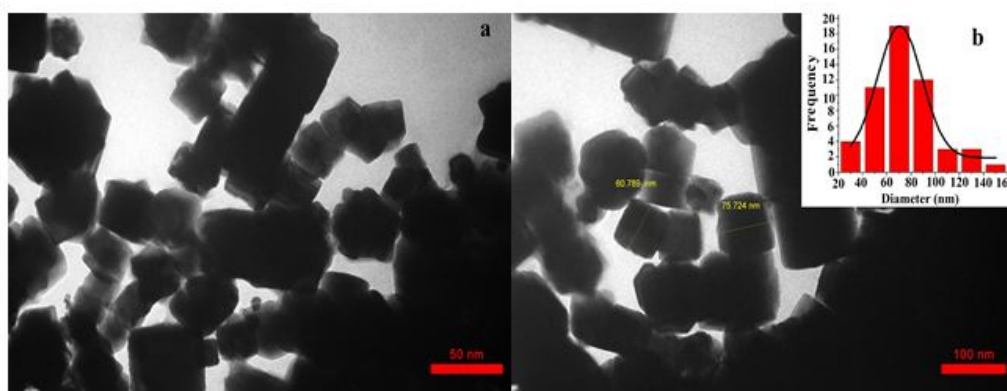


Figure 6. TEM images at different scale bars: (a) 50 nm, (b) 100 nm, of Fe_3O_4 @APTES-TA-MA.

The XRD pattern of the Fe_3O_4 @APTES nanoparticles shows six peaks at 30.04° , 35.5° , 43.1° , 53.4° , 57.0° , and 62.6° , which are related to the (220), (311), (400), (422), (511) and (440) reflection planes of Fe_3O_4 (JCPDS NO.75-1609), respectively. These six typical peaks could be also found in the XRD patterns of the Fe_3O_4 @APTES-TA-MA, indicating that the main crystal phase structure of Fe_3O_4 @APTES is maintained after covalent organic framework conjugation.

To receive the best reaction conditions, the reaction of 4-Cl-benzaldehyde, malononitrile and cyanoacetohydrazide was studied as a sample reaction in different solvents. The results illustrated that Fe_3O_4 @APTES-TA-MA is more effective in EtOH as a polar protic solvent at reflux condition than the yield and the reaction time of received product (Table 1). The high catalytic performance of the catalyst in EtOH (96%) can be ascribed to the better deprotonation of the malononitrile by Fe_3O_4 @APTES-TA-MA in the polar protic solvent. To study of the efficiency of the catalyst, the sample reaction was also applied with different amounts of Fe_3O_4 @APTES-TA-MA. The result showed that the best amount of Fe_3O_4 @APTES-TA-MA was 0.04 g, which provided the needed product with high efficiency (Table 1, entry 3).

After obtaining the best reaction conditions, a variety of N-amino-2-pyridone analogs was produced by Fe_3O_4 @APTES-TA-MA with high yield (Table 2, entries 1-12). As can be seen from Table 2, electron withdrawing groups in aldehyde derivatives can improve the activity

of the reactants (Table 2, entries 1-6). Also, we tested n-butanal as an aliphatic aldehyde and furfural as a hetero aldehyde in the reaction. Due to low reactivity of aliphatic aldehyde and side reactions of furfural, the results were unsuccessful.

The possible mechanism with Fe_3O_4 @APTES-TA-MA as an magnetic COF nanocatalyst is presented in Scheme 3. The reaction maybe proceeds via the initial Knoevenagel condensation between malononitrile and arylaldehyde in the presence of Fe_3O_4 @APTES-TA-MA to generate the intermediate I by dehydration. The intermediate I then undergoes Michael addition with activated cyanoacetohydrazide, and the intermediate II is produced. Then, intramolecular cyclization of intermediate II underwent tautomerization of the resulting intermediate III which undergoes dehydration to form N-amino-2-pyridones V.

To investigate the efficiency of the present method for the production of N-amino-2-pyridones, the construction of compound 4a was compared with some cases reported in the literature (Table 2). It is evident from the results that Fe_3O_4 @APTES-TA-MA provides excellent yield in reducing the reaction time.

Furthermore, the leaching of the nanocatalyst was investigated with the hot filtration test. The reaction of 4-Cl-benzaldehyde, malononitrile, and cyanoacetohydrazide at the presence of nanocatalyst was stopped after 5 min and the nanocatalyst filtered from the reaction mixture. The filtrate was heated and the reaction followed and checked with thin layer chromatography. The reaction did not progress

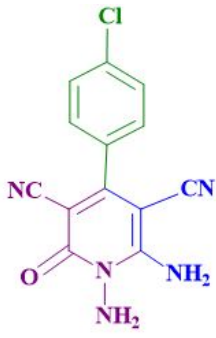
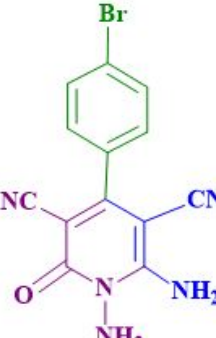
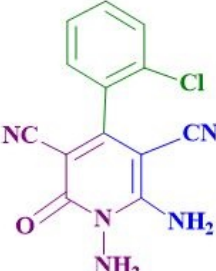
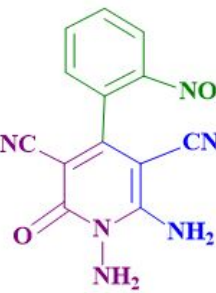
Table 1. Construction of 4a in different solvents and different amounts of the catalyst^a.

entry	solvent	yield (%) ^b	catalyst (g)	yield (%) ^b
1	EtOAc	45	0.02	85
2	EtOH (96%)	97	0.03	90
3	MeOH	86	0.04	97
5	MeCN	70	0.05	97
6	CHCl_3	40	-	-

^a Reaction conditions: 4-Cl-benzaldehyde (1 mmol), malononitrile (1 mmol), and cyanoacetohydrazide (1 mmol), at reflux temperature after 25 min.

^b Separated yields.

Table 2. Synthesis of N-amino-2-pyridone analogs by Fe₃O₄@APTES-TA-MA^a.

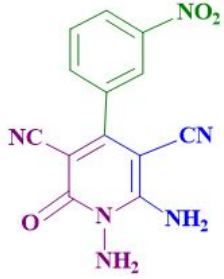
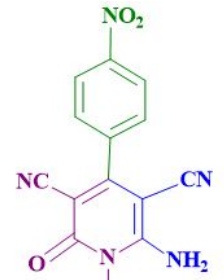
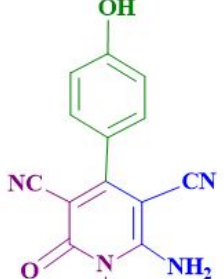
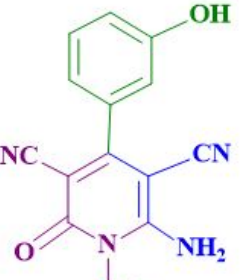
entry	X	product	time (min)	yield (%) ^b	mp (°C)	ref.
1	4-Cl	 4a	25	97	243-245	242-243 [35]
2	4-Br	 4b	25	96	236-238	234-236 [35]
3	2-Cl	 4c	30	94	302-304	305-307 [33]
4	2-NO ₂	 4d	30	95	232-234	234-236 [35]

^a Reaction conditions: malononitrile (1 mmol), cyanoacetohydrazide (1 mmol), aldehyde (1 mmol), Fe₃O₄@APTES-TA-MA (0.04 g), ethanol (5 ml) at reflux temperature.

^b All yields refer to isolated products.

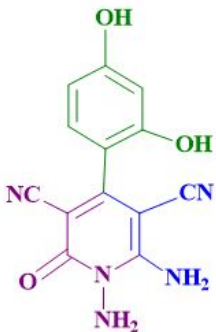
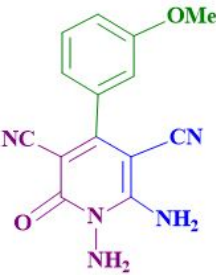
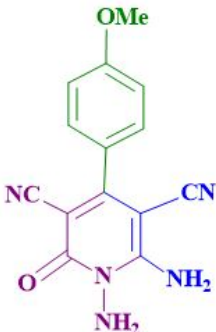
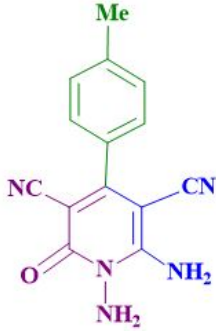
Continued on next page

Table 2. Synthesis of N-amino-2-pyridone analogs by Fe₃O₄@APTES-TA-MA^a. (Continued)

entry	product	time (min)	yield (%)	mp (°C)	mp [Lit] (°C)	
5	3-NO ₂  4e		30	94	240-242	-
6	4-NO ₂  4f		25	98	228-230	226-228 [35]
7	4-OH  4g		45	89	>300	325-327 [41]
8	3-OH  4h		45	90	256-258	-

Continued on next page

Table 2. Synthesis of N-amino-2-pyridone analogs by Fe₃O₄@APTES-TA-MA^a. (Continued)

entry	product	time (min)	yield (%)	mp (°C)	mp [Lit] (°C)
9	2,4-(OH) ₂  4i		50	87	261-263
10	3-MeO  4j		45	89	263-265 265-267 [33]
11	4-MeO  4k		45	90	222-224 222-224 [35]
12	4-Me  4l		45	88	239-240 238-240 [35]

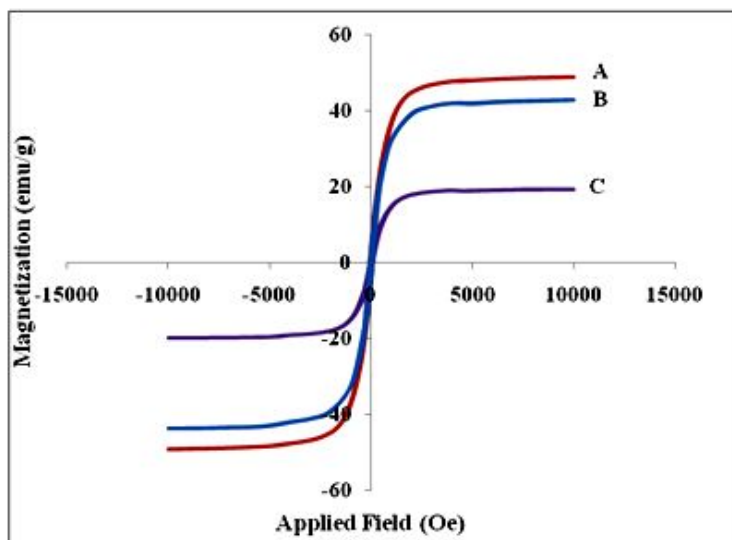


Figure 7. VSM image of Fe_3O_4 NPs (A), Fe_3O_4 @APTES NPs (B) and Fe_3O_4 @APTES-TA-MA (C) nanocatalyst.

after filtration, so the negative consequences of hot filtration test show that the leaching of nanocatalyst is insignificant. To evaluate the recyclability of Fe_3O_4 @APTES-TA-MA, it was used in the production of 4a, five cycles under the optimal conditions. The Fe_3O_4 @APTES-TA-MA catalyst was reused through simple filtration and washed with CH_2Cl_2 . Then, according to the amount of the catalyst, the required amount of fresh cyanoacetohydrazide, 4-Cl-benzaldehyde and malononitrile was added. The results

showed that Fe_3O_4 @APTES-TA-MA can be recycled five times without decreasing its catalytic activity efficiency (Fig. 9).

4. Conclusion

In conclusion, the conjugation of covalent organic framework on Fe_3O_4 @APTES gives a heterogeneous, green and recyclable magnetic covalent organic framework nanocatalyst for the one-pot production of N-amino-2-pyridones via

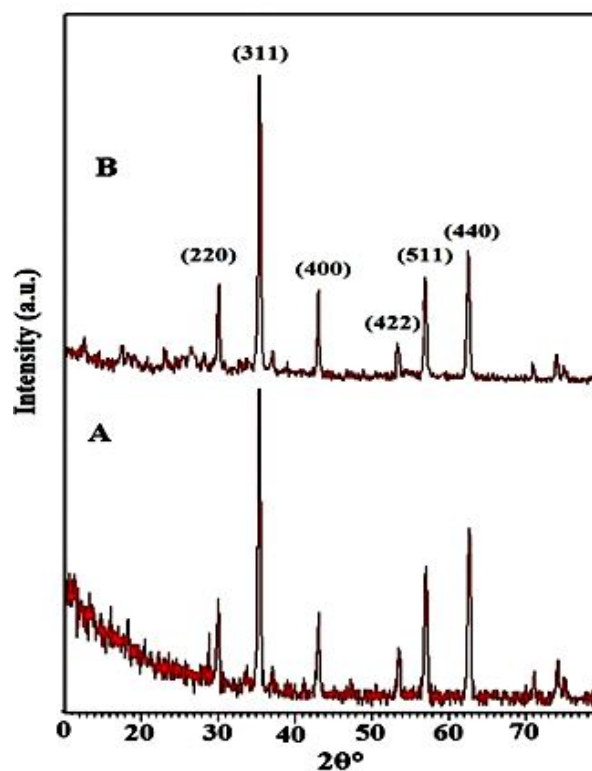
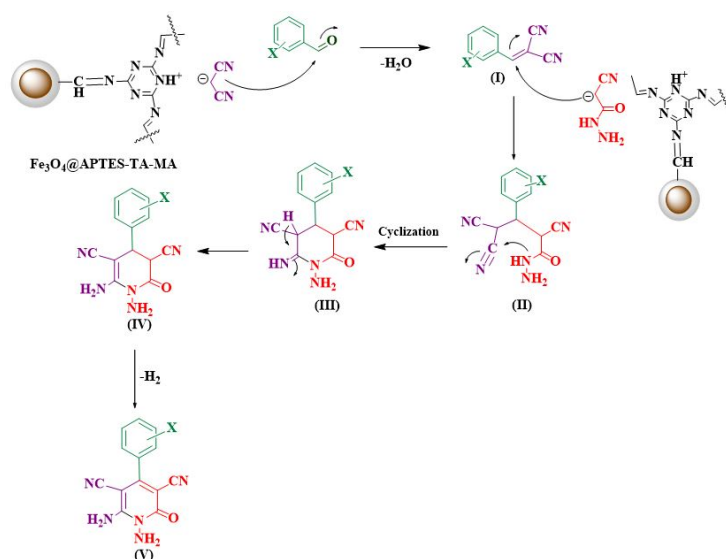


Figure 8. XRD diffraction patterns: A) Fe_3O_4 @APTES, B) Fe_3O_4 @APTES-TA-MA nanocatalyst.



Scheme 3. Reaction pathway proposed for the production of N-amino-2-pyridone analogs by $\text{Fe}_3\text{O}_4@APTES\text{-TA-MA}$.

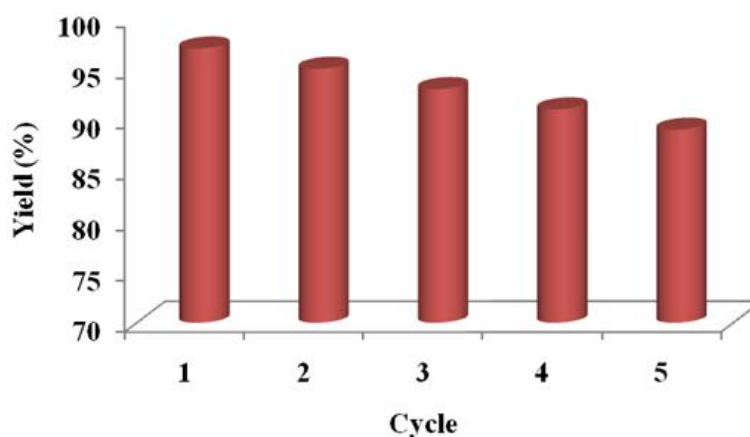


Figure 9. Reusability of $\text{Fe}_3\text{O}_4@APTES\text{-TA-MA}$ in the synthesis of product 4a.

the reaction of arylaldehyde, malononitrile and cyanoacetohydrazide in EtOH at reflux conditions. High yields, simple work-up procedure and no side reactions are some benefits of this method. It is clear that the unique magnetic properties of the superparamagnetic particles lead to recyclable magnetic nanoparticles immobilized with covalent organic framework for several times using a suitable magnet with no significant loss in their catalytic activity. The sustainable synthesis of magnetically retrievable covalent organic framework using readily available reactants will also make this field of research green. Additional interesting development is the covalent organic framework stabilized magnetic nanoparticles as a new group of heterogeneous nanocatalyst that is mainly attractive in organic synthesis practiced in an environmentally friendly approach. In the end, future efforts for more efficient protocols will continue to focus on the stability, sustainability, environmental impact and significant cost and energy savings due to growing needs of industry. These efforts enable a wide variety of industrial applications for the covalent organic framework immobilized on magnetic nanoparticles in the future.

Ethical Approval

This manuscript does not report on or involve the use of any animal or human data or tissue. So the ethical approval does not applicable.

Authors Contributions

All authors have contributed equally to prepare the paper.

Availability of Data and Materials

The data that support the findings of this study are available from the corresponding author upon reasonable request.

Conflict of Interests

The authors declare that they have no known competing financial interests or personal relationships that could have appeared to influence the work reported in this paper.

Open Access

This article is licensed under a Creative Commons Attribution 4.0 International License, which permits use, sharing, adaptation, distribution and reproduction in any medium or format, as long as you give appropriate credit to the original author(s) and the source, provide a link to the Creative Commons license, and indicate if changes were made. The images or other third party material in this article are included in the article's Creative Commons license, unless indicated otherwise in a credit line to the material. If material is not included in the article's Creative Commons license and your intended use is not permitted by statutory regulation or exceeds the permitted use, you will need to obtain permission directly from the OICCPress publisher. To view a copy of this license, visit <https://creativecommons.org/licenses/by/4.0>.

References

- [1] A.P. Côté, A.I. Benin, N.W. Ockwig, M. O'Keefe, A.J. Matzger, and O.M. Yaghi. Crystalline, covalent organic frameworks. *Science*, **310**:1166–1170, 2005. DOI: <https://doi.org/10.1126/science.1120411>.
- [2] H.M. El-Kaderi, J.R. Hunt, A.P. Mendoza-Cortez, A.P. Côté, R.M. Taylor, M. O'Keefe, and O.M. Yaghi. Designed synthesis of 3D covalent organic frameworks. *Science*, **316**:268–272, 2007. DOI: <https://doi.org/10.1126/science.1139915>.
- [3] S. Shylesh, V. Schünemann, and W.R. Thiel. Magnetically separable nanocatalysts: bridges between homogeneous and heterogeneous catalysis. *Angew. Chem. Int. Ed.*, **49**:3428–3459, 2010. DOI: <https://doi.org/10.1002/anie.200905684>.
- [4] M. Mokhtary. Recent advances in catalysts immobilized on magnetic nanoparticles. *J. Iran. Chem. Soc.*, **13**:1827–1845, 2016. DOI: <https://doi.org/10.1007/s13738-016-0900-4>.
- [5] T. Cheng, D. Zhang, H. Li, and G. Liu. Magnetically recoverable nanoparticles as efficient catalysts for organic transformations in aqueous medium. *Green Chem.*, **16**:3401, 2014. DOI: <https://doi.org/10.1039/c4gc00458b>.
- [6] Z.Q. Liu, Y.Y. Yu, Y.J. Liu, A.G. Ying, X.L. Zhang, and Y. Wang. Unlocking birch lignin hydrocracking through tandem catalysis: unraveling the role of moderate hydrogen spillover. *ACS Catal.*, **14**:2115–2126, 2024. DOI: <https://doi.org/10.1021/acscatal.3c04721>.
- [7] F. Rezaei, H. Alinezhad, and B. Maleki. Captopril supported on magnetic graphene nitride, a sustainable and green catalyst for one-pot multicomponent synthesis of 2-amino-4H-chromene and 1,2,3,6-tetrahydropyrimidine. *Sci. Rep.*, **13**:20562, 2023. DOI: <https://doi.org/10.1038/s41598-023-47794-2>.
- [8] H. Atharifar, A. Keivanloo, B. Maleki, M. Baghayeri, and H. Alinezhad. Magnetic nanoparticle supported choline chloride-glucose (deep eutectic solvent) for the one-pot synthesis of 3,4-disubstituted isoxazol-5(4H)-ones. *Res. Chem. Intermed., Inpress*, **50**:281–296, 2024. DOI: <https://doi.org/10.1007/s11164-023-05152-x>.
- [9] A. Gholami, M. Mokhtary, S.S. Attarseyedi, B. Masoumi, and M. Mamaghani. Synthesis of polyfunctionalized furan analogs catalyzed by chlorosulfonic acid immobilized nano-cobaltferrite. *J. Clust. Sci.*, **35**:69–78, 2024. DOI: <https://doi.org/10.1007/s10876-023-02462-3>.
- [10] N. Azgomi and M. Mokhtary. Nano-Fe₃O₄@SiO₂ supported ionic liquid as an efficient catalyst for the synthesis of 1,3-thiazolidin-4-ones under solvent-free conditions. *J. Mol. Catal. A: Chem.*, **398**:58–64, 2015. DOI: <https://doi.org/10.1016/j.molcata.2014.11.018>.
- [11] B. Babaei, M. Mamaghani, and M. Mokhtary. Sustainable approach to the synthesis of 1,4-disubstituted triazoles using reusable Cu(II) complex supported on hydroxyapatite-encapsulated α -Fe₂O₃ as organic-inorganic hybrid nanocatalyst. *React. Kinet. Mech. Catal.*, **128**:379–394, 2019. DOI: <https://doi.org/10.1007/s11144-019-01636-3>.
- [12] S. Vajjar and M. Mokhtary. Nano-CuFe₂O₄@SO₃H catalyzed efficient one-pot cyclo-dehydration of dimedone and synthesis of chromeno[4,3-b]chromenes. *Polycycl. Aromat. Compd.*, **39**:111–123, 2019. DOI: <https://doi.org/10.1080/10406638.2017.1280516>.
- [13] M. Dashti, M. Nikpassand, M. Mokhtary, and L. Zare Fekri. Fe₃O₄@SP@Chitosan@Fe₃O₄ nanocomposite: A catalyst with double magnetite parts for sustainable synthesis of novel azo-linked 4-benzylidene-2-phenyloxazol-5-ones. *Polycycl. Aromat. Compd.*, **43**:4889–4905, 2023. DOI: <https://doi.org/10.1080/10406638.2022.2097714>.
- [14] M. Dashti, M. Nikpassand, M. Mokhtary, and L. Zare Fekri. Sustainable synthesis of azo-linked 4-arylidene-2-aryloxazolones using Fe₃O₄@SiPr@vanillin@TGA nanocomposite. *J. Clust. Sci.*, **34**:1037–1049, 2023. DOI: <https://doi.org/10.1007/s10876-022-02279-6>.
- [15] A. Gholami, M. Mokhtary, and M. Nikpassand. Glycolic acid-supported cobalt ferrite-catalyzed one-pot synthesis of pyrimido[4,5-b]quinoline and indenopyrido[2,3-d]pyrimidine derivatives. *Appl. Organomet. Chem.*, **34**:e6007, 2020. DOI: <https://doi.org/10.1002/aoc.6007>.
- [16] M. Foroughi Kaldareh, M. Mokhtary, and M. Nikpassand. Nicotinic acid-supported cobalt ferrite-catalyzed one-pot synthesis of substituted chromeno[3,4-b]quinolines. *Appl. Organomet. Chem.*, **34**:e5469, 2020. DOI: <https://doi.org/10.1002/aoc.5469>.

- [17] A. Ying, S. Li, X. Liu, J. Wang, Y. Liu, and Z. Liu. Fabrication of DABCO functionalized poly(ionic liquids): Vital role of ferric oxides in the formation of mesoporous structure and used as highly efficient and recyclable catalysts for multi-component reactions. *J. Catal*, **391**:312–326, 2020. DOI: <https://doi.org/10.1016/j.jcat.2020.08.031>.
- [18] X. Lu, S. Li, L. Wang, S. Huang, Z. Liu, Y. Liu, and A. Ying. Novel photic and magnetic double responsive Pickering interfacial solid catalysts for biodiesel production. *Fuel*, **310**:122318, 2022. DOI: <https://doi.org/10.1016/j.fuel.2021.122318>.
- [19] S. Li, X. Lu, Q. Liu, L. Wang, Y. Liu, Z. Liu, and A. Ying. Template-free fabrication of magnetic mesoporous poly(ionic liquid)s: efficient interfacial catalysts for hydrogenation reaction and transesterification of soybean oil. *J. Mater. Chem. A*, **10**:3531–3542, 2022. DOI: <https://doi.org/10.1039/D1TA09265K>.
- [20] L.A. Mitscher. Bacterial topoisomerase inhibitors: quinolone and pyridone antibacterial agents. *Chem. Rev*, **105**:559–592, 2005. DOI: <https://doi.org/10.1021/cr030101q>.
- [21] M.T. Cocco, C. Congiu, V. Onnis, M. Morelli, and O. Cauli. Synthesis of ibuprofen heterocyclic amides and investigation of their analgesic and toxicological properties. *Eur. J. Med. Chem*, **38**:513–518, 2003. DOI: [https://doi.org/10.1016/s0223-5234\(03\)00074-6](https://doi.org/10.1016/s0223-5234(03)00074-6).
- [22] A.G.E. Amr and M.M. Abdulla. Anti-inflammatory profile of some synthesized heterocyclic pyridone and pyridine derivatives fused with steroidal structure. *Bioorg. Med. Chem*, **14**:4341–4352, 2006. DOI: <https://doi.org/10.1016/j.bmc.2006.02.045>.
- [23] I.V. Magedov, M. Manpadi, N.M. Evdokimov, E.M. Elias, E. Rozhkova, M.A. Ogasawara, J.D. Bettale, N.M. Przheval'skii, S. Rogelj, and A. Kornienko. Antiproliferative and apoptosis inducing properties of pyrano[3,2-c]pyridones accessible by a one-step multicomponent synthesis. *Bioorg. Med. Chem. Lett*, **17**:3872–3876, 2007. DOI: <https://doi.org/10.1016/j.bmcl.2007.05.004>.
- [24] F. Wei, D. Kang, S. Cherukupalli, W.A. Zalloum, T. Zhang, X. Liu, and P. Zhan. Discovery and optimizing polycyclic pyridone compounds as anti-HBV agents. *Expert Opin. Ther. Pat*, **30**:715–721, 2020. DOI: <https://doi.org/10.1080/13543776.2020.1801641>.
- [25] K.L. Forrestall, D.E. Burley, M.K. Cash, I.R. Potte, and S. Darvesh. 2-Pyridone natural products as inhibitors of SARS-CoV-2 main protease. *Chem. Biol. Interact*, **335**:109348, 2021. DOI: <https://doi.org/10.1016/j.cbi.2020.109348>.
- [26] G. Öztürk, D.D. Erol, T. Uzbay, and M.D. Aytemir. Synthesis of 4(1H)-pyridinone derivatives and investigation of analgesic and anti-inflammatory activities. *Farmaco*, **56**:251–256, 2001. DOI: [https://doi.org/10.1016/s0014-827x\(01\)01083-7](https://doi.org/10.1016/s0014-827x(01)01083-7).
- [27] J.G. Sos'nicki and T.J. Idzik. Pyridones—powerful precursors for the synthesis of alkaloids, their derivatives, and alkaloid-inspired compounds. *Synthesis*, **51**:3369–3396, 2019. DOI: <https://doi.org/10.1055/s-0037-1611844>.
- [28] R.A. Azzam and G.H. Elgemeie. Design and synthesis of a new class of pyridine-based N-sulfonamides exhibiting antiviral, antimicrobial, and enzyme inhibition characteristics. *Med. Chem. Res*, **28**:62–70, 2019. DOI: <https://doi.org/10.1021/acsomega.0c03773>.
- [29] H. Hosseini and M. Bayat. Cyanoacetylhydrazides in synthesis of heterocyclic compounds. *Top. Curr. Chem*, **376**:40, 2018. DOI: <https://doi.org/10.1007/s41061-018-0218-z>.
- [30] M. Haffas, N. Benkiki, R. Maadadi, O. Talhi, C. Boukentoucha, F. Chebrouk, and Z. Kabouche. In Situ one pot Hemi-Synthesis of New 2-Pyridone Derivatives. *Chem. Proc*, **3**, 2021. DOI: <https://doi.org/10.3390/ecsoc-25-11724>.
- [31] D.L. Comins, X. Chen, and S.P. Joseph. Synthesis of 2,4-disubstituted N-acyl-5,6-dihydro-2-pyridones. *Tetrahedron Lett*, **37**:9275–9278, 1996. DOI: [https://doi.org/10.1016/S0040-4039\(97\)82940-1](https://doi.org/10.1016/S0040-4039(97)82940-1).
- [32] M. Seifi, M. Khajehasani Rabori, and H. Sheibani. Highly efficient method for synthesis of N-amino-2-pyridone derivatives in the presence of catalysts such as magnesium oxide (MgO) and bismuth(III) nitrate pentahydrate (Bi(NO₃)₃·5H₂O). *Mod. Res. Catal*, **2**:8, 2013. DOI: <https://doi.org/10.4236/mrc.2013.22A002>.
- [33] H. Hosseini and M. Bayat. An efficient and ecofriendly synthesis of highly functionalized pyridones via a one-pot three-component reaction. *RSC Adv*, **8**:27131, 2018. DOI: <https://doi.org/10.1039/c8ra05690k>.
- [34] M.R. Mahmoud and F.S.M. Abu El-Azm. Synthesis and spectral studies of novel heterocycles from 2-cyano-N'-(9H-fluoren-9-ylidene) acetylhydrazide. *Eur. Chem. Bull*, **2**:335–340, 2013. DOI: <https://doi.org/10.17628/ECB.2013.2.335>.
- [35] J. Safaei-Ghomi, H. Shahbazi-Alavi, and A. Ziarati. A comparative screening of the catalytic activity of nanocrystalline M_{II}Zr₄(PO₄)₆ ceramics in the one-pot synthesis of 1,6-diamino-4-aryl-2-oxo-1,2-dihydropyridine-3,5-dicarbonitrile derivatives. *Res. Chem. Intermed*, **43**:91–101, 2017. DOI: <https://doi.org/10.1007/s11164-016-2608-6>.
- [36] B. Kshiar, O.R. Shangpliang, and B. Myrboh. A three component one-pot synthesis of N-amino-2-pyridone derivatives catalyzed by KF-Al₂O₃.

- Synth. Commun.*, **48**:1816–1827, 2018. DOI: <https://doi.org/10.1080/00397911.2018.1468467>.
- [37] J. Safaei-Ghomi, M.R. Saberi-Moghadam, H. Shahbazi-Alavi, and M. Asgari-Kheirabadi. An efficient method for the synthesis of N-amino-2-pyridones using reusable catalyst ZnO nanoparticles. *J. Chem. Res.*, **38**:583–585, 2014. DOI: <https://doi.org/10.3184/174751914X14109743944>.
- [38] A. Mosaffaeirad, M. Mokhtary, and M. Nikpassand. PVPP-p-TSA catalyzed one-step synthesis of novel aryldiazenyl-2-hydroxybenzylidene-cyanoarylhydrazide analogs. *J. Mol. Struct.*, **1293**:136227, 2023. DOI: <https://doi.org/10.1016/j.molstruc.2023.136227>.
- [39] M. Pourmohammad and M. Mokhtary. K₂CO₃-catalyzed synthesis of 2-amino-3-cyano-4H-chromene derivatives with different substituents in water. *C. R. Chimie*, **18**:554–557, 2015. DOI: <https://doi.org/10.1016/j.crci.2014.09.008>.
- [40] E. Zare and Z. Rafiee. Magnetic chitosan supported covalent organic framework/copper nanocomposite as an efficient and recoverable catalyst for the unsymmetrical hantzsch reaction. *J. Taiwan Inst. Chem. Eng.*, **116**:205–214, 2020. DOI: <https://doi.org/10.1016/j.jtice.2020.10.028>.
- [41] S. Babae, M. Zarei, H. Sepehrmansourie, M.A. Zolfigol, and S. Rostamnia. Synthesis of metal-organic frameworks MIL-101(Cr)-NH₂ containing phosphorous acid functional groups: application for the synthesis of N-amino-2-pyridone and pyrano[2,3-c]pyrazole derivatives via a cooperative vinylogous anomeric-based oxidation. *ACS Omega*, **5**:6240–6249, 2020. DOI: <https://doi.org/10.1021/acsomega.9b02133>.